ACS MEASUREMENT SCIENCE Au
AN OPEN ACCESS JOURNAL OF THE AMERICAN CHEMICAL SOCIETY

pubs.acs.org/measureau
Article

Legion: An Instrument for High-Throughput Electrochemistry

Benjamin H. R. Gerroll, Krista M. Kulesa, Charles A. Ault, and Lane A. Baker*

Cite This: ACS Meas. Sci. Au 2023, 3, 371−379
Read Online

ABSTRACT: Electrochemical arrays promise utility for accelerated hypothesis testing and breakthrough discoveries. Herein, we report a new high-throughput electrochemistry platform, colloquially called "Legion," for applications in electroanalysis and electrosynthesis. Legion consists of 96 electrochemical cells dimensioned to match common 96-well plates that are independently controlled with a field-programmable gate array. We demonstrate the utility of Legion by measuring model electrochemical probes, pH-dependent electron transfers, and electrocatalytic dehalogenation reactions. We consider advantages and disadvantages of this new instrumentation, with the hope of expanding the electrochemical toolbox.

KEYWORDS: *electrochemistry, voltammetry, instrumentation, array, high throughput*

INTRODUCTION

Discovery and analysis with array-based measurements is an important approach in modern measurement science. For instance, arrays of biomolecules, such as nucleic acids or peptides, have proven to be key tools in genomics, proteomics, molecular biology, and bioinformatics.[1−4] Likewise, arrays based on chemical properties, such as ligand identity,[5] nanoparticle type,[6] and metallic compositions,[7] have found utility in the discovery of new synthetic routes,[8] catalysts,[9,10] and metamaterials.[11] Signal detection/transduction in array-based measurements has been dominated by optical methods, where fluorescence is especially adept. Array analysis by mass spectrometry has also contributed to significant discoveries, especially in the realm of biomolecules where libraries produced with molecular biology tools find great utility. While electrochemical arrays have also found application in synthesis and reaction screening,[12−15] far fewer commercial systems are available. Applications of hardware for electrochemical research have been developed for the last several decades and were recently reviewed extensively.[16] Electrochemical arrays often consist of a single type of electrode arrayed and biased at a common potential and take advantage of mass transport effects to the array. Parallel approaches where each electrode in an array can be operated at the same time with independent control of potential and signal collection have been much less common, owing largely to difficulties in instrumentation. To enable truly high-throughput electrochemistry, we believe arrays of electrochemical cells should ideally operate with full, simultaneous control over each electrode. Applications of a parallel high-throughput electrochemical cell array could find impact over a broad range of science, including electro-organic synthesis,[17−20] electrocatalyst discovery, fundamental nanoscience, and bioelectrochemical assays.

High-throughput electrochemical measurements can be performed serially or in parallel. An automated platform for the serial investigation of structure−function relationships in substituted oligothiophenes was described by Briehn *et al.*[21] A microtiter plate, set on a mobile stage able to move in $x-y$ directions, was placed under a three-electrode bundle moved by an automated z-positioning controller. The electrode bundle was lowered into individual microwells repeatedly to carry out sequential experiments in each well of the microtiter plate. This configuration evaluates different solution conditions and electrochemical parameters in a single experimental setup, using a single potentiostat. However, to avoid cross contamination, at least every other well must be a "wash" well, limiting the number of conditions that can be tested. Furthermore, since each condition is tested serially, a comprehensive evaluation takes considerable time.

Parallel experiments conduct an array of electrochemical measurements simultaneously. For example, the electrocatalytic activity of platinum deposited on 64 individual glassy carbon electrodes was tested simultaneously by Hayden *et al.*[22] A single potentiostat was connected to a 64-channel current

Received: May 13, 2023
Revised: June 27, 2023
Accepted: June 28, 2023
Published: July 13, 2023

https://doi.org/10.1021/acsmeasuresciau.3c00022
ACS Meas. Sci. Au 2023, 3, 371−379

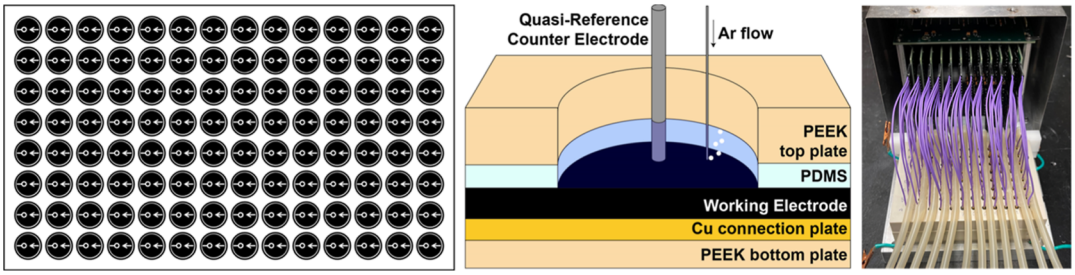

Figure 1. Layout of electrochemical cell array, where the dimensions of the array match a standard 96-well plate (left). Cartoon of a single electrochemical cell in the array. Each cell is 7 mm in diameter and contains up to 500 μL of solution (middle). Photograph of the instrument. Purple wires are leads from the QRCE to internal circuitry. Yellow tubes deliver sparging gas to each cell (right).

follower to allow all working electrodes to function at the same time. However, all working electrodes were configured in a common electrolyte bath and subjected to the same potential waveform. While this enables screening of many working electrodes at once, only a single substrate or reagent in the common electrolyte can be explored at a time. Furthermore, applied experimental potentials are limited without individual control over each electrode. For typical formats, achieving individual control over the potential or current applied to an array of working electrodes requires an equal number of dedicated potentiostats or galvanostats.

To this end, multi-channel multiplexed potentiostats/galvanostats have been employed to improve throughput. Ley *et al.* electrochemically and spectroscopically screened 8 wells of a 24-well microtiter plate simultaneously.[23] This approach drew on a well-plate footprint utilized in combinatorial electrochemistry, for sequential measurements of potassium ferrocyanide and decoloration of the dye indigo carmine. However, measurements remain serial and were limited in scale by dedicated instrumentation.

Within the realm of synthetic and preparative scale reactions, Rein *et al.*[24] described a system capable of incorporating both electrochemistry and photochemistry into a high-throughput framework. Their design, also based on a standard 24-well microtiter plate, provides unique customizability with a modular design and the possibility of scale-up to 96 wells. Moreover, each row of the 4 × 6 plate can be independently controlled. However, this system does not allow for individual control over the potential in each well. Gütz *et al.*[25] achieved individual control over 8 distinct electrochemical cells through a standard 8-channel galvanostat. Despite the advantages of this approach, increasing throughput requires the costly addition of dedicated galvanostats.

Precedent emphasizes the need for high-throughput electrochemical instrumentation operating (i) with individually addressable working electrodes, (ii) in isolated solution environments simultaneously, and (iii) with simplified electrode design. Additionally, a geometric footprint compatible with standard microtiter plates is desirable to facilitate integration into existing frameworks of spectroscopic and mass-spectrometric high-throughput analysis. Here, we describe a new electrochemical platform, colloquially referred to as "Legion", which improves throughput with parallel electrochemical cell arrays. In the present iteration, electrochemical cells in the array operate in an undivided configuration and can carry out 96 individual experiments effectively and simultaneously in a footprint that matches a standard 96-well plate. General instrumental construction, performance benchmarks, and preliminary applications are described. Instrument benchmarking is discussed in the context of three well-established redox mediators: potassium ferricyanide, ruthenium hexaammine, and ferrocenemethanol. Screening capabilities are demonstrated by replicating measurements of proton and electron transfer by anthraquinone-2,6-disulfonate across a broad pH range.[26] Screening and synthetic capabilities of Legion are then demonstrated in the context of electrochemical reduction of halogenated acetamides and halogenated octanes.

EXPERIMENTAL SECTION

Instrument Design

To facilitate future post-electrochemical analysis, the layout of the electrochemical cells was dimensioned to match a standard 96-well microtiter plate, with individual cells arranged in a 12 × 8 format (Figure 1, right). The electrochemical cell array consists of a machined polyether ether ketone (PEEK) top, a polydimethylsiloxane (PDMS) gasket, a glassy carbon plate working electrode, a copper base plate for electrical connection, and a bottom PEEK plate (Figure 1, middle). The entire assembly is joined with compression provided by four machine screws at each corner. The PEEK top plate primarily defines the solution volume of each electrochemical cell. The exposed electrode area at the bottom of each electrochemical cell is 7 mm in diameter (28.3 mm^2). Each cell holds a maximum volume of 500 μL, although practical operating volumes in the present design can be as low as 200 μL. A quasi-reference counter electrode (QRCE) is present in each electrochemical cell, with composition as described for each specific experiment (typically Ag/AgCl or Ag/AgO). For measurements reported here, solution volumes of 300 μL, with QRCE electroactive surface areas of approximately 35 mm^2 were used.

Each QRCE is connected to the instrument *via* pin connectors that lead to custom circuitry and electronics for the potentiostat (Figure 1, left). Eight QRCEs in each column are connected *via* pin connectors to an 8-channel potentiostat board. The twelve 8-channel potentiostat boards interface with a field programmable gate array (FPGA). The potential at each QRCE can be individually controlled and the current flowing through each QRCE is independently measured. For a single electrochemical cell, a control potential for the reference electrode channel is used to set the QRCE. Current through the QRCE is measured across a sensing resistor in the counter electrode channel. Data are stored by the FPGA and relayed to the control computer at specified intervals. Custom instrument software developed in LabVIEW and FPGA-specific software allows for the application of swept, complex, or stepped potential waveforms. As configured here, the instrument has a voltage range of ±4 V and a current range of ±250 μA with an 8 nA resolution. Electrochemical data were processed using Python.

Sparging of solution and thereby convection can be achieved with a tubing manifold that splits a single gas source into 96 outlets by means of a reducing splitter, and twelve rubber hoses. Each hose contains 8 evenly spaced 23-gauge needles sealed to the hose with

https://doi.org/10.1021/acsmeasuresciau.3c00022
ACS Meas. Sci. Au 2023, 3, 371−379

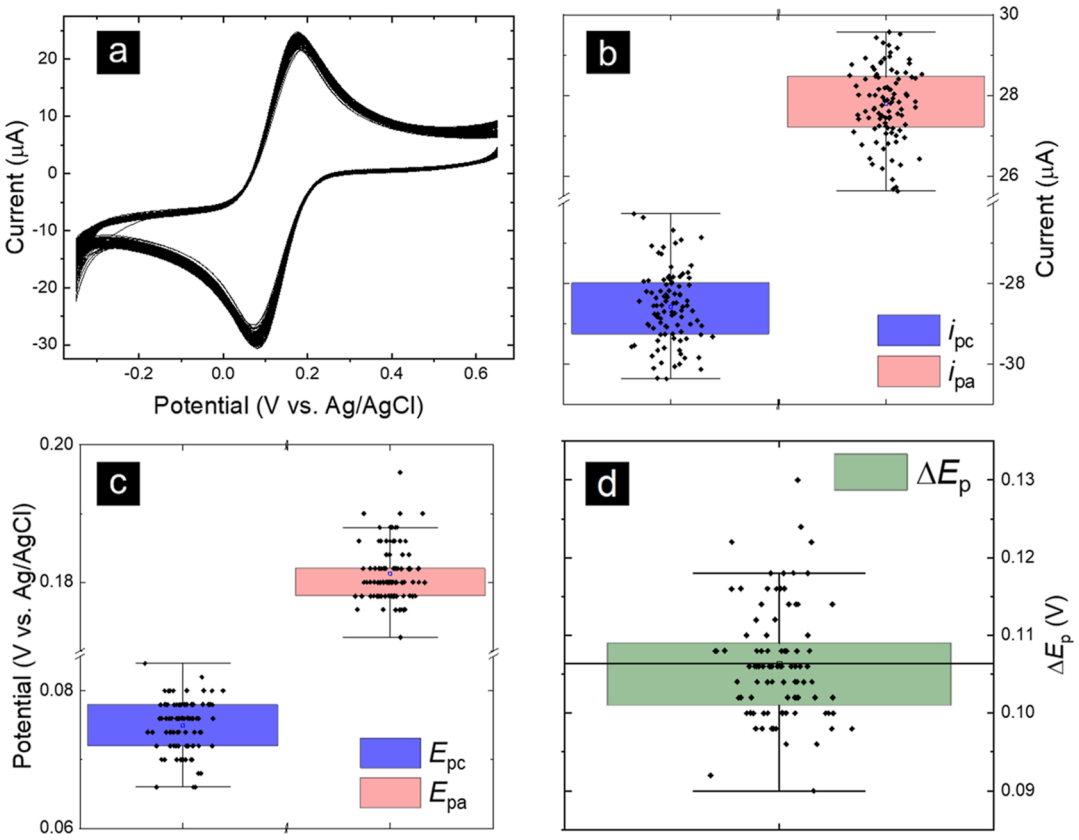

Figure 2. (a) Ninety-six simultaneous cyclic voltammograms recorded at 100 mV/s for a 0.5 mM solution of $K_3Fe(CN)_6$ in 0.1 M aqueous KCl. Scan rate achieved with E_{step} and t_{step} values of 2 mV and 0.02 s, respectively. (b) Cathodic peak current (i_{pc}, black symbols blue shading) and anodic peak current (i_{pa}, black symbols red shading) measured for each voltammogram. (c) Cathodic peak potential (E_{pc}, black symbols blue shading) and anodic peak potential (E_{pa}, black symbols red shading) currents as measured from an extrapolated baseline for each voltammogram. (d) Potential difference between measured peak cathodic and peak anodic potentials.

flexible silicone epoxy. Needles can be placed into each electrochemical cell of the array as desired.

Reagents

The following chemicals were used as received unless otherwise stated: potassium ferricyanide (EMD chemicals, >99.0%), hexaammineruthenium(III) chloride (Strem Chemicals, 99%), ferrocenemethanol (Strem Chemicals, 99%), anthraquinone-2,6-disulfonic acid disodium salt (Combi-Blocks, 98%), potassium chloride (Fisher Chemical, >99.0%), potassium phosphate dibasic (J.T. Baker, 99.6%), potassium phosphate monobasic (Fisher Chemical, 99.3%), sodium carbonate (Sigma-Aldrich, 99.5+%), sodium bicarbonate (Fisher Chemical, >99.7%), citric acid monohydrate (Mallinckrodt, 99.6%), potassium carbonate (VWR, 99.0%), dodecane (Sigma-Aldrich, 99+%), 2-iodo-*N*-methylacetamide (IMA; Princeton Biopharma), 2-iodo-*N*,*N*-dimethylacetamide (IDMA; Enamine Ltd, 91%), 1-iodooctane (IO; Sigma-Aldrich, 98%), 1,8-diiodooctane (DIO; Sigma-Aldrich, 98%), 2-iodo-*N*-phenylacetamide (IPA; Ark Pharm, 95+%), and 2-bromo-*N*-phenylacetamide (BPA; Oakwood Chemical, 98%). All water was purified in a Millipore purification system to a specific resistance of 18.3 MΩ cm. Tetramethylammonium tetrafluoroborate ($TMABF_4$; TCI, 98%) was recrystallized from water and methanol and stored under vacuum at 80 °C overnight prior to use as a non-aqueous electrolyte.

Electrodes

A glassy carbon plate (redox.me, 110 mm × 73 mm × 3 mm) functioned as the working electrode. Before assembling the electrochemical cell array plate, the glassy carbon was sequentially polished on a MasterTex Buehler polishing pad with alumina slurries decreasing in size from 0.3 to 0.05 μm. In between each polishing step, the glassy carbon was sonicated in isopropyl alcohol with activated carbon as previously described.[27] After the final polishing step, the plate was sonicated in isopropyl alcohol/activated carbon, followed by sonication in an anticipated experimental solvent.

Silver wire (Millipore Sigma, 1 mm diameter, 99.9%) was cut into 25 mm length pieces for the QRCEs. Wires were briefly sanded to remove surface oxides, then immersed in a solution of 1 M $FeCl_3$ in 1 M HCl for 5 s each, to generate a surface layer of AgCl for aqueous measurements. Silver oxide QRCEs were employed for non-aqueous experiments. The surface of each silver wire was sanded, then briefly dipped in concentrated nitric acid. Unless otherwise stated, potentials herein are reported with respect to the Ag/AgCl QRCE. Post-electrolysis electrodes were rinsed with common solvents and wiped clean for preparation for reuse.

Electrolyte Solutions

For electrochemical measurements of anthraquinone-2,6-disulfonate over a broad range of pH values, aqueous solutions of 0.1 M KCl at pH = 1 (HCl), pH = 3 (0.1 M citric acid), pH = 4−5 (0.05 M acetic acid, 0.05 M sodium acetate), pH = 6−8 (0.05 M potassium phosphate monobasic, 0.05 M potassium phosphate dibasic), pH = 9−10 (0.05 M sodium carbonate, 0.05 M sodium bicarbonate), pH = 11 (0.1 M sodium carbonate), and pH = 12 (KOH) were prepared. Solutions were adjusted to the desired pH by addition of HCl or KOH. For electrochemical measurements of halogenated acetamides at pH = 4, pH = 6, and pH = 8, aqueous solutions of 0.05 M potassium phosphate monobasic with 0.1 M KCl were prepared and adjusted to the desired pH with HCl or KOH.

Separation, Identification, and Quantitation of Electrolysis Products

Electrolysis products were identified by means of gas chromatography−mass spectrometry (GC−MS). An Agilent 6130 gas chromato-

https://doi.org/10.1021/acsmeasuresciau.3c00022
ACS Meas. Sci. Au 2023, 3, 371−379

graph with a 30 m × 0.32 mm, 5% phenylpolysiloxane, and 95% methylpolysiloxane DB-5 capillary column (J&W Scientific) was employed in tandem with an Agilent 5973 inert mass-selective detector operating in an electron ionization mode (70 eV). Major products were quantified by means of GC. Solution in each cell was partitioned between 1 mL of ethyl acetate containing 1 mM *n*-dodecane as an internal standard and water, then subsequently washed three times with water. The organic phase was then injected onto an Agilent 7890A gas chromatograph equipped with a flame-ionization detector and a 30 m × 0.25 mm capillary column (J&W Scientific) with a DB-5 stationary phase consisting of 5% phenyl-polysiloxane and 95% methylpolysiloxane. Chromatographic peak areas were integrated with respect to the *n*-dodecane internal standard. Established procedures were used to quantitate products on the basis of GC.[28]

RESULTS AND DISCUSSION

To establish baseline performance, 96 simultaneous cyclic voltammograms of potassium ferricyanide, $K_3Fe(CN)_6$, were recorded (Figure 2a). All recorded cyclic voltammograms display reversible electron transfer, with average cathodic (E_{pc}) and anodic (E_{pa}) peak potentials measured at 0.075 ± 0.004 and 0.182 ± 0.004 V, respectively, after background current subtraction. The observed cathodic and anodic peak separation (ΔE_p) of 107 mV is larger than the expected value of 59 mV for an electrochemically reversible one-electron process. However, the ratio of cathodic peak current (i_{pc}) to anodic peak current (i_{pa}) is 1.03 ± 0.01. Box-whisker plots (Figure 2b–d) illustrate the precision of electrochemical measurements. Of 96 measured E_{pc} values (Figure 2c, gray box), no outliers are recorded below the 5th percentile or above the 95th percentile. However, several E_{pa} values are measured at potentials more positive than the 95th percentile. Despite this variation in E_{pa}, both i_{pc} and i_{pa} (Figure 2b) measurements fall within the lower 5th and upper 95th percentiles. The peak current ratio can also be used to assess electrochemical reversibility (as opposed to ΔE_p), further illustrated by the appearance of outliers in Figure 2d. Variations observed in standard cyclic voltammetry (CV) may arise from several factors. First, the size of the glassy carbon plate is quite large and may possess inherent heterogeneity in conductivity or differences in sheet resistance may contribute to slight differences in cell potentials. We would note, however, that with a backing copper plate, systematic variations in electrochemical cell performance were not observed based on the location of the electrochemical cell in the array. Second, these experiments have 96 individual QRCEs which possess inherent variability. Third, the electrochemical cell geometry is nonideal as boundary conditions for solution concentrations are not uniform with the geometry employed. The ratio of the working electrode area to QRCE area for each individual cell is close to unity, an obviously nonideal situation for stable potential measurement. Despite these caveats, we believe the 96-well format of Legion provides promising advantages in compatibility with other platforms.

Additional benchmarking of electrochemical performance was carried out to further validate Legion. To examine the possibility of electrochemical contamination across wells, three separate 0.5 mM solutions of $K_3Fe(CN)_6$, ferrocenemethanol (FcMeOH), and ruthenium hexaammine ($[Ru(NH_3)_6]Cl_3$) in 0.1 M KCl supporting electrolyte were prepared. All three of these redox reagents are known to support reversible, one-electron transfers. Each solution was pipetted into alternating columns (Figure 3, inset). Different potential sweep windows were necessary to measure each $E_{1/2}$.

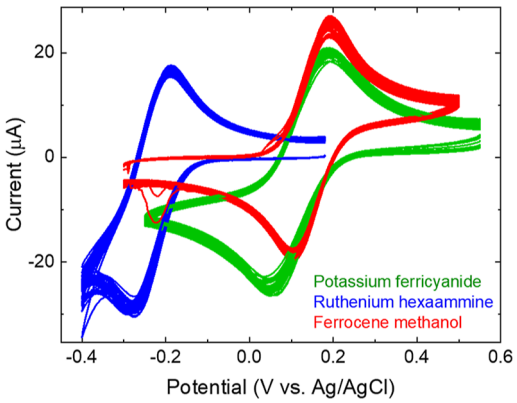

Figure 3. Cyclic voltammograms recorded simultaneously at the glassy carbon electrode at 100 mV/s in aqueous solutions containing 0.1 M KCl, 0.5 mM potassium ferricyanide (black), 0.5 mM ruthenium hexaammine (blue), and ferrocenemethanol (red). Inset: well plate map showing location of each solution. Scan rate achieved with E_{step} and t_{step} values of 2 mV and 0.02 s, respectively.

Cells containing $K_3Fe(CN)_6$ (Figure 3, green) were swept from 0.55 to −0.035 V, then back to 0.55 V. An electrochemically reversible one-electron reduction is observed, with average E_{pc} and E_{pa} values, respectively, measured at 0.051 and 0.191 V, ±0.006 V. The average ratio of i_{pc} to i_{pa} is 0.96, with standard deviations in cathodic and anodic peak currents of 0.9 and 1.1 μA, respectively. Though ΔE_p is 140 mV, a peak current ratio of 0.96 indicates electrochemical reversibility.

Cyclic voltammograms of $[Ru(NH_3)_6]Cl_3$ (Figure 3, blue) were recorded by sweeping the potential from 0.18 to −0.40 V, then back to 0.18 V. The cathodic sweep shows a single E_{pc} at −0.279 V for one-electron reduction, followed by a single E_{pa} at −0.189 V in the anodic return sweep. The ratio of i_{pc} to i_{pa} is 2.59, which is larger than expected for an electrochemically reversible process; however, the peak splitting is only 90 mV. As solutions in this particular experiment were not degassed, the abnormal peak current ratio is likely due to the presence of trace oxygen in solution that undergoes reduction at *ca.* −0.40 V. The presence of this side reaction results in an inflated cathodic peak current and unreliable baselines for measurement of anodic peak currents.

Cyclic voltammograms of FcMeOH (Figure 3, red) were recorded by sweeping the potential from −0.030 to 0.050 V, then back to −0.030 V, affording one reversible electron transfer. Average peak potentials are measured at 0.189 V (E_{pa}) and 0.104 V (E_{pc}), with an average separation of 85 mV. Average peak current ratios are found to be 0.90, which supports electrochemical reversibility of arrayed $[FcMeOH]^0/[FcMeOH]^+$.

Of note, smaller standard deviations in peak currents are measured during the forward sweep when compared to the return sweep for all three substrates. This difference in precision occurs regardless of initial potential bias. No difference in the precision of peak potential measurements is observed.

The ability to perform 96 simultaneous electrochemical reactions was additionally demonstrated in scan rate-dependent electrode responses of $K_3Fe(CN)_6$, $[Ru(NH_3)_6]Cl_3$, and

https://doi.org/10.1021/acsmeasuresciau.3c00022
ACS Meas. Sci. Au 2023, 3, 371−379

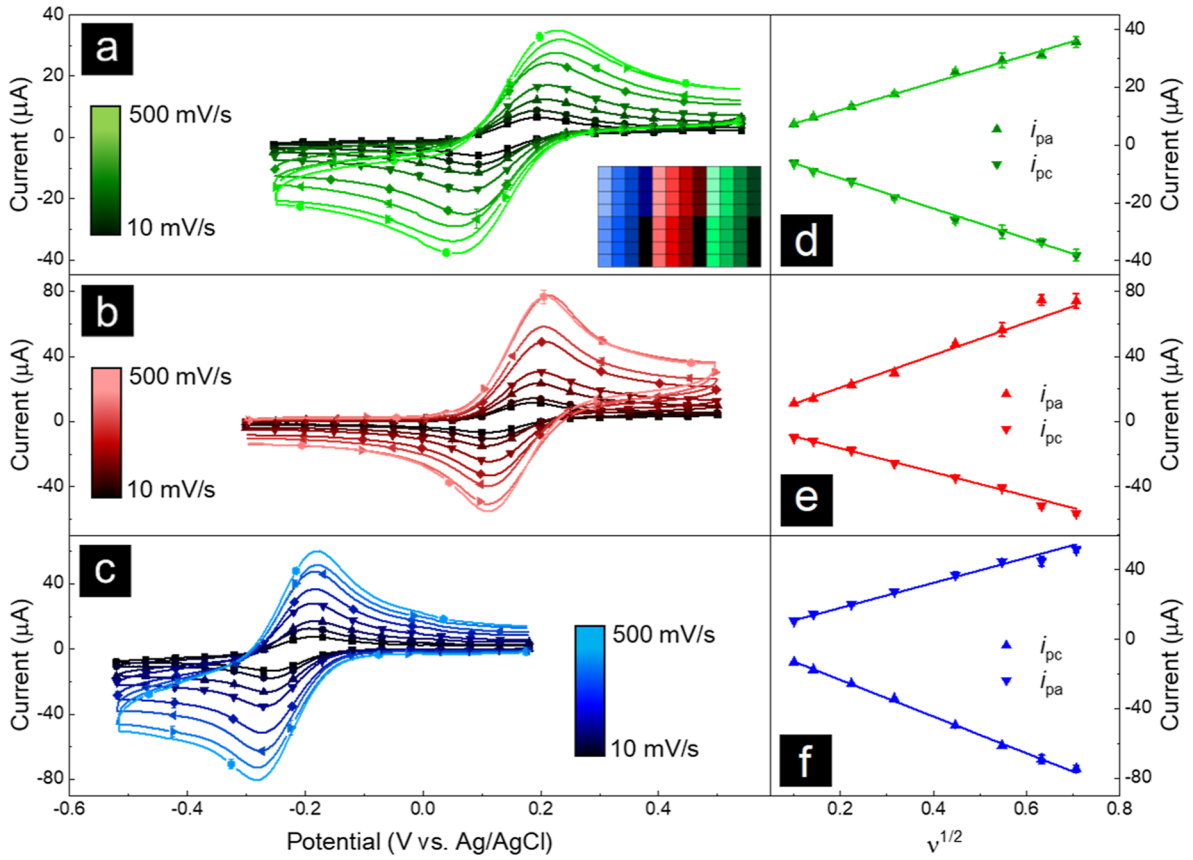

Figure 4. Averaged cyclic voltammograms recorded at 10, 20, 50, 100, 200, 300, 400, and 500 mV/s of 0.5 mM solutions of (a) $K_3Fe(CN)_6$, (b) $[Ru(NH_3)_6]Cl_3$, and (c) FcMeOH in 0.1 M KCl supporting electrolyte. Peak currents measured from corresponding cyclic voltammograms of (d) $K_3Fe(CN)_6$, (e) $[Ru(NH_3)_6]Cl_3$, and (f) FcMeOH plotted as a function of $\nu^{1/2}$ for calculation of diffusion coefficients. The inset in panel (a) illustrates the location of each substrate in the instrument. Scan rate is correlated to shade, with lightest color shading representing 10 mV/s and darkest representing 500 mV/s.

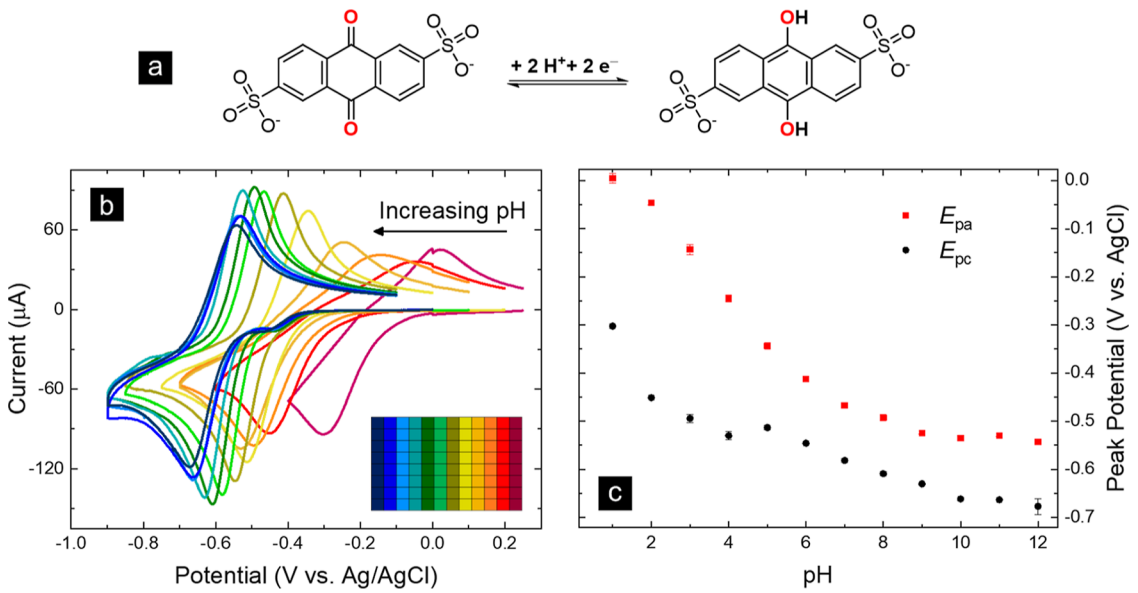

Figure 5. (a) Scheme for electrochemical reduction of AQDS. (b) Averaged cyclic voltammograms collected at an electrochemical cell array with the glassy carbon working electrode of 1 mM AQDS in 0.1 M KCl buffered to pH = 1, 3, 4, 5, 6, 7, 8, 9, 10, 11, 12, and 13. Each voltammogram is an average of eight cyclic voltammograms collected at each pH. Inset: well plate map of each pH solution, with pH = 1 in the farthest right column (dark gray) to pH = 13 in the farthest left column (orange). (c) Anodic and cathodic peak potentials measured as a function of pH.

FcMeOH. Solutions of 0.5 mM $K_3Fe(CN)_6$ (red), $[Ru(NH_3)_6]Cl_3$ (blue), and FcMeOH (green) were arrayed in 0.1 M KCl supporting electrolyte (Figure 4a–c). Four cyclic voltammograms at each scan rate were recorded for each

https://doi.org/10.1021/acsmeasuresciau.3c00022
ACS Meas. Sci. Au 2023, 3, 371–379

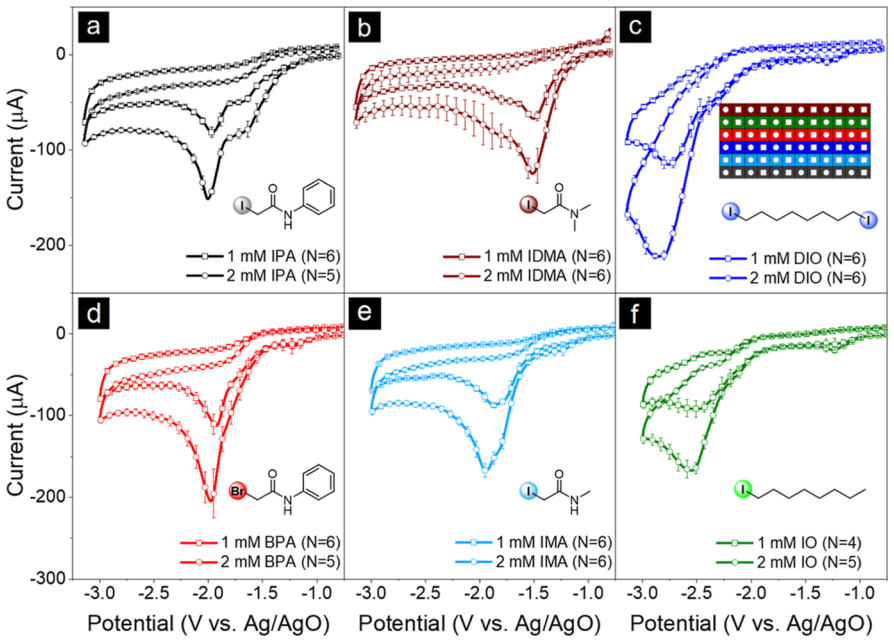

Figure 6. Averaged cyclic voltammograms recorded at 100 mV/s at electrochemical cell array with the glassy carbon electrode for 1 mM (-□-) and 2 mM (-○-) concentrations of (a) IPA, (b) IDMA, (c) DIO, (d) BPA, (e) IMA, and (f) IO in DMF containing 0.1 M $TMABF_4$. Inset in (c) is a map of conditions for each electrochemical cell (top and bottom rows are not shown as they contained only 0.1 M $TMABF_4$ to collect background cyclic voltammograms).

substrate. For each of the three substrates, cathodic and anodic peak currents increase as the scan rate increases. Anodic peak potentials shift toward more positive values as scan rate increases across all substrates. However, E_{pa} stabilizes after 400 mV/s in the case of $K_3Fe(CN)_6$. Cathodic peak potentials shift to more negative potentials for 0.5 mM $K_3Fe(CN)_6$ and 0.5 mM $[Ru(NH_3)_6]Cl_3$, once again stabilizing after 400 mV/s in the case of $K_3Fe(CN)_6$. Interestingly, for 0.5 mM FcMeOH, no shift in cathodic peak potential is observed. Plots of cathodic and anodic peak current with respect to the square root of scan rate ($\nu^{1/2}$) show linear relationships for $K_3Fe(CN)_6$, $[Ru(NH_3)_6]Cl_3$, and FcMeOH (Figure 4d–f). Diffusion coefficients calculated from these data are smaller than values reported in the literature (Table S1, Supporting Information),[29,30] which highlights a shortcoming of the present hardware configuration. Low diffusion coefficients are a consequence of the relatively large peak separations and are likely further exacerbated by discrepancy between the cell geometry and/or the active area of the working electrode relative to the assumed geometric surface area.[31]

pH-Dependent Electrochemical Measurements

Anthraquinone-2,6-disulfonate (AQDS) has previously been employed for the electrochemical detection of DNA.[32] Reduction of AQDS proceeds by a $2H^+$, $2e^-$ transfer pathway, and is thus influenced by solution pH (Figure 5). At low pH, the quinone moiety is protonated (chemical, *C* step), followed by electrochemical reduction (electrochemical, *E* step) (Figure 5a). This occurs twice to fully reduce AQDS, following a *CECE* pathway. Batchelor-McAuley *et al.*[26] investigated the electrochemical behavior of AQDS and anthraquinone-2-disulfonate from pH = 1 through pH = 12 *via* CV, describing the $2H^+$, $2e^-$ transfer through a square scheme.

A sequential voltammetric study of electrochemical behavior across a wide pH range requires individual electrochemical cells for each buffered condition. High-throughput analysis with Legion offers a more efficient approach to fundamental but experimentally time-consuming questions such as coupled H^+/e^- transfers. Simultaneous measurements at 96 independent electrochemical cells can rapidly screen pH conditions and study proton-dependent electron transfer observed in AQDS in a single experimental setup.

Cyclic voltammograms of 1 mM AQDS at 100 mV/s were recorded in all 96 wells. In an acidic electrolyte, AQDS demonstrates quasi-reversible electron transfer and reversibility increases with pH (Figure 5b). In low pH arrays, the reaction proceeds *via* the previously observed *CECE* pathway, wherein the quinone moiety is protonated before electron transfer. Figure 5c shows the average peak potentials measured at each pH and changes in electrochemical reversibility observed over the pH range studied. This pH-dependent electron-transfer behavior is in good agreement with the original mechanism proposed by Batchelor-McAuley *et al.*[26]

Electrochemical Screening and Bulk Electrolysis of Halogenated Species

High-throughput, independently controlled sweep methods are crucial for analytical electrochemical studies. However, the ability to step and hold a unique potential in each of the 96 cells increases the number of electrosynthetic and preparative scale reactions that can be performed at one time. To these points, the electrochemical reduction of several halogenated compounds was investigated by CV, followed by high-throughput controlled potential electrolysis and offline product analysis, to learn about reaction viability, mechanism, and optimization. To examine this closely, we drew from previous demonstrations of electrochemical dehalogenation reactions of Peters and co-workers.[33] Six organic substrates were selected for electrochemical dehalogenation: IPA, BPA, IDMA, IMA, IO, and DIO.

Electrochemical reduction of 1 and 2 mM substrate concentrations was first investigated by recording cyclic

https://doi.org/10.1021/acsmeasuresciau.3c00022
ACS Meas. Sci. Au 2023, 3, 371−379

Table 1. Product Quantitation for Bulk Reduction of Reactions Described

			% yield[a]					
substrate	E (V vs AgO)	c (mM)	DIO	IO	octane	BPA	IPA	PA
DIO	−2.8	1	TR[b]	TR[b]	15			
		0.5	TR[b]	TR[b]	19			
	−2.3	1	TR[b]	TR[b]	13			
		0.5	TR[b]	TR[b]	20			
IO	−2.75	2		TR[b]	11			
		1		TR[b]	9			
	−2.3	2		TR[b]	7			
		1		TR[b]	10			
BPA	−2.2	2				TR[b]		50
		1				TR[b]		54
	−1.8	2				TR[b]		39
		1				TR[b]		40
IPA	−2.2	2					TR[b]	41
		1					TR[b]	41
	−1.65	2					TR[b]	49
		1					TR[b]	34

[a]Yield expressed as the percentage of the substrate appearing as each compound relative to the added internal standard. [b]TR = a trace amount (<1%) was detected but not quantitated.

voltammograms at a glassy carbon electrode in DMF solutions containing 0.1 M $TMABF_4$ supporting electrolyte at a sweep rate of 100 mV/s. In the case of all six substrates, averaged cyclic voltammograms show irreversible cathodic processes generated by the cleavage of carbon−halogen bonds (Figure 6). In some substrates, additional cathodic processes are observed. Reduction of IPA produces two cathodic processes at −1.50 and −1.80 V *vs* the Ag/AgO QRCE (Figure 6a). Similarly, reduction of the brominated analogue, BPA, generates a large wave at −1.90 V *vs* Ag/AgO with a small cathodic shoulder at 1.72 V *vs* Ag/AgO (Figure 6d). Reduction of IDMA (Figure 6b) generates a single cathodic wave at −1.42 V *vs* Ag/AgO. However, IMA (Figure 6e) presents two broader cathodic waves at *ca.* −1.80 and −1.90 V *vs* Ag/AgO. Reduction of DIO (Figure 6c) produces a small, broad cathodic wave at −2.20 V and a large wave at −2.72 V *vs* Ag/AgO. Reduction of IO (Figure 6f) shows similar electrochemical behavior, with approximately half of the cathodic current relative to DIO. This is likely because there is only one cleavable C−X bond in IO. The presence of multiple peaks observed for the phenylacetamides (Figure 6a,d) has been previously ascribed to the possibility of deprotonation of the amide nitrogen forming an anionic species that is reduced at more negative potentials, with adventitious water serving as a possible hydroxide source.[34,35] The presence of multiple cathodic peaks observed during reduction of IMA (Figure 6e), and not for IDMA (Figure 6b), lends evidence for this mechanism, although other possible pathways, such as amide-iminol tautomerization upon reduction, cannot be explicitly ruled out.

Averaged voltammograms were used as guides for selecting bulk electrolysis potentials. Substrates BPA, IPA, IO, and DIO were chosen to directly compare (i) the halogen, (ii) the degree of halogenation, and (iii) substituent effects. Substrates were arrayed on the instrument in two different concentrations. Since BPA, IPA, IO, and DIO all demonstrated two mechanistically relevant cathodic waves, each substrate was electrolyzed at two different applied potentials based on CV data. Table 1 provides the potential at which electrolysis processes were conducted, and the amount of *n*-octane, or phenylacetamide (PA) quantitated. In all cases, the amount of starting material remaining in solution was ≤2%. With only *ca.* 50% recovery of phenylacetamide, no other products were detected despite previous reports of cyclized products.[34,35] Reduction of IO and DIO at all concentrations and potentials provided octane as the major product. Smaller amounts of 1-octanol, 1-octene, hexadecane, and cyclooctane were detected but not quantitated as expected from previous reports on electrochemical reduction of primary iodoalkanes.[36,37] These bulk electrolysis results obtained with Legion are in excellent agreement with the literature and demonstrate its ability to screen electrochemical properties and electrosynthetic transformations with unprecedented throughput and control.

CONCLUSIONS

Legion is an electrochemical cell array that boosts throughput of electrochemical experimentation allowing the opportunity to conduct 96 independent electrochemical experiments simultaneously. The design, modeled around commercially available 96-well plates, enables facile integration with existing frameworks for high-throughput analysis. Reliability and reproducibility are demonstrated through cyclic voltammograms of the well-established and extensively characterized redox systems potassium ferricyanide, ruthenium hexaammine, and ferrocenemethanol. The 96-cell design allows for collection of replicate data sets to maintain statistical significance. Replication of two studies requiring two different electrochemical methods showcases the ability to reproduce previously published results in an arrayed format. We believe Legion will find future application in a number of studies for electroanalysis and electrosynthesis. Future studies will consider consequences of and possible improvements to the undivided cell format,[38] integration with complementary high-throughput analysis formats, and utilization of statistical approaches that this array format can enable.[39]

https://doi.org/10.1021/acsmeasuresciau.3c00022
ACS Meas. Sci. Au 2023, 3, 371−379

■ ASSOCIATED CONTENT

Supporting Information

The Supporting Information is available free of charge at https://pubs.acs.org/doi/10.1021/acsmeasuresciau.3c00022.

Calculated diffusion coefficients and controlled potential electrolysis experimental results (PDF)

■ AUTHOR INFORMATION

Corresponding Author

Lane A. Baker − *Department of Chemistry, Texas A&M University, College Station, Texas 77843, United States;* orcid.org/0000-0001-5127-507X; Email: lane.baker@tamu.edu

Authors

Benjamin H. R. Gerroll − *Department of Chemistry, Indiana University, Bloomington, Indiana 47405, United States*

Krista M. Kulesa − *Department of Chemistry, Indiana University, Bloomington, Indiana 47405, United States; Department of Chemistry, Texas A&M University, College Station, Texas 77843, United States*

Charles A. Ault − *Department of Chemistry, Indiana University, Bloomington, Indiana 47405, United States*

Complete contact information is available at: https://pubs.acs.org/10.1021/acsmeasuresciau.3c00022

Author Contributions

CRediT: **Benjamin H R Gerroll** conceptualization (lead), data curation (lead), formal analysis (lead), investigation (equal), methodology (equal), resources (equal); **Krista M Kulesa** data curation (equal), formal analysis (equal), writing-review & editing (equal); **Charles A Ault** investigation (supporting); **Lane A Baker** conceptualization (equal), formal analysis (equal), funding acquisition (lead), investigation (equal), methodology (equal), project administration (lead), supervision (lead), writing-review & editing (lead).

Notes

The authors declare no competing financial interest.

■ ACKNOWLEDGMENTS

Financial support of the American Chemical Society Petroleum Research Fund (PRF#62019-NDS), the National Science Foundation Center for Single-Entity Nanochemistry and Nanocrystal Design (CHE 2221062), Texas A&M University, and Indiana University are acknowledged. Electronic Instrument Services and Mechanical Instrument Services at Indiana University are acknowledged.

■ REFERENCES

(1) Blay, V.; Tolani, B.; Ho, S. P.; Arkin, M. R. High-Throughput screening: Today's biochemical and cell-based approaches. *Drug Discovery Today* **2020**, *25*, 1807−1821.

(2) Yang, L.; Pijuan-Galito, S.; Rho, H. S.; Vasilevich, A. S.; Eren, A. D.; Ge, L.; Habibovic, P.; Alexander, M. R.; de Boer, J.; Carlier, A.; van Rijn, P.; Zhou, Q. High-throughput methods in the discovery and study of biomaterials and materiobiology. *Chem. Rev.* **2021**, *121*, 4561−4677.

(3) Soheilmoghaddam, F.; Rumble, M.; Cooper-White, J. High-throughput routes to biomaterials discovery. *Chem. Rev.* **2021**, *121*, 10792−10864.

(4) Inglese, J.; Auld, D. S.; Jadhav, A.; Johnson, R. L.; Simeonov, A.; Yasgar, A.; Zheng, W.; Austin, C. P. Quantitative high-throughput screening: A titration-based approach that efficiently identifies biological activities in large chemical libraries. *Proc. Natl. Acad. Sci. U.S.A.* **2006**, *103*, 11473−11478.

(5) Renom-Carrasco, M.; Lefort, L. Ligand libraries for high throughput screening of homogeneous catalysts. *Chem. Soc. Rev.* **2018**, *47*, 5038−5060.

(6) Chan, E. M. Combinatorial approaches for developing upconverting nanomaterials: high-throughput screening, modeling, and applications. *Chem. Soc. Rev.* **2015**, *44*, 1653−1679.

(7) Yao, Y.; Huang, Z.; Li, T.; Wang, H.; Liu, Y.; Stein, H. S.; Mao, Y.; Gao, J.; Jiao, M.; Dong, Q.; Dong, Q.; et al. High-throughput, combinatorial synthesis of multimetallic nanoclusters. *Proc. Natl. Acad. Sci. U.S.A.* **2020**, *117*, 6316−6322.

(8) Jäkel, C.; Paciello, R. High-throughput and parallel screening methods in asymmetric hydrogenation. *Chem. Rev.* **2006**, *106*, 2912−2942.

(9) Isbrandt, E. S.; Sullivan, R. J.; Newman, S. G. High throughput strategies for the discovery and optimization of catalytic reactions. *Angew. Chem., Int. Ed.* **2019**, *58*, 7180−7191.

(10) Robbins, D. W.; Hartwig, J. F. A simple, multidimensional approach to high-throughput discovery of catalytic reactions. *Science* **2011**, *333*, 1423−1427.

(11) Plum, E.; Tanaka, K.; Chen, W. T.; Fedotov, V. A.; Tsai, D. P.; Zheludev, N. I. A combinatorial approach to metamaterials discovery. *J. Opt.* **2011**, *13*, 055102.

(12) Xu, X.; Valavanis, D.; Ciocci, P.; Confederat, S.; Marcuccio, F.; Lemineur, J.-F.; Actis, P.; Kanoufi, F.; Unwin, P. R. The new era of high-throughput nanoelectrochemistry. *Anal. Chem.* **2023**, *95*, 319−356.

(13) Feng, E.; Jing, Q.; Moeller, K. D. Lessons from an array: Using an electrode surface to control selectivity of a solution-phase chemical reaction. *Angew. Chem., Int. Ed.* **2022**, *61*, No. e202116351.

(14) Alden, S. E.; Siepser, N. P.; Patterson, J. A.; Jagdale, G. S.; Choi, M.; Baker, L. A. Array microcell method (AMCM) for serial electroanalysis. *ChemElectroChem* **2020**, *7*, 1061−1091.

(15) Pence, M. A.; Rodríguez, O.; Lukhanin, N. G.; Schroeder, C. M.; Rodríguez-López, J. Automated measurement of electrogenerated redox species degradation using multiplexed interdigitated electrode arrays. *ACS Meas. Sci. Au* **2023**, *3*, 62−72.

(16) Wills, A. G.; Charvet, S.; Battilocchio, C.; Scarborough, C. C.; Wheelhouse, K. M. P.; Poole, D. L.; Carson, N.; Vantourout, J. C. High-Throughput Electrochemistry: State of the Art, Challenges, and Perspective. *Org. Process Res. Dev.* **2021**, *25*, 2587−2600.

(17) Yan, M.; Kawamata, Y.; Baran, P. S. Synthetic organic electrochemical methods since 2000: on the verge of a renaissance. *Chem. Rev.* **2017**, *117*, 13230−13319.

(18) Francke, R.; Little, R. D. Redox catalysis in organic electrosynthesis: basic principles and recent developments. *Chem. Soc. Rev.* **2014**, *43*, 2492−2521.

(19) Leech, M. C.; Garcia, A. D.; Petti, A.; Dobbs, A. P.; Lam, K. Organic electrosynthesis: from academia to industry. *React. Chem. Eng.* **2020**, *5*, 977−990.

(20) Shatskiy, A.; Lundberg, H.; Kärkäs, M. D. Organic electrosynthesis: applications in complex molecule synthesis. *ChemElectroChem* **2019**, *6*, 4067−4092.

(21) Briehn, C. A.; Schiedel, M. S.; Bonsen, E. M.; Schuhmann, W.; Bäuerle, P. Single-Compound Libraries of Organic Materials: From the Combinatorial Synthesis of Conjugated Oligomers to Structure−Property Relationships. *Angew. Chem., Int. Ed.* **2001**, *40*, 4680−4683.

(22) Guerin, S.; Hayden, B. E.; Lee, C. E.; Mormiche, C.; Owen, J. R.; Russell, A. E.; Theobald, B.; Thompsett, D. Combinatorial electrochemical screening of fuel cell electrocatalysts. *J. Comb. Chem.* **2004**, *35*, 149−158.

(23) Ley, C.; Zengin Çekiç, S.; Kochius, S.; Mangold, K.-M.; Schwaneberg, U.; Schrader, J.; Holtmann, D. An electrochemical microtiter plate for parallel spectroelectrochemical measurements. *Electrochim. Acta* **2013**, *89*, 98−105.

(24) Rein, J.; Annand, J. R.; Wismer, M. K.; Fu, J.; Siu, J. C.; Klapars, A.; Strotman, N. A.; Kalyani, D.; Lehnherr, D.; Lin, S. Unlocking the Potential of High-Throughput Experimentation for Electrochemistry with a Standardized Microscale Reactor. *ACS Cent. Sci.* **2021**, *7*, 1347−1355.
(25) Gütz, C.; Klöckner, B.; Waldvogel, S. R. Electrochemical screening for electroorganic synthesis. *Org. Process Res. Dev.* **2016**, *20*, 26−32.
(26) Batchelor-McAuley, C.; Li, Q.; Dapin, S. M.; Compton, R. G. Voltammetric characterization of DNA intercalators across the full pH range: Anthraquinone-2, 6-disulfonate and anthraquinone-2-sulfonate. *J. Phys. Chem. B* **2010**, *114*, 4094−4100.
(27) Ranganathan, S.; Kuo, T.-C.; McCreery, R. L. Facile preparation of active glassy carbon electrodes with activated carbon and organic solvents. *Anal. Chem.* **1999**, *71*, 3574−3580.
(28) Pritts, W. A.; Vieira, K. L.; Peters, D. G. Quantitative determination of volatile products formed in electrolyses of organic compounds. *Anal. Chem.* **1993**, *65*, 2145−2149.
(29) Moldenhauer, J.; Meier, M.; Paul, D. W. Rapid and direct determination of diffusion coefficients using microelectrode arrays. *J. Electrochem. Soc.* **2016**, *163*, H672−H678.
(30) Miao, W.; Ding, Z.; Bard, A. J. Solution Viscosity Effects on the Heterogeneous Electron Transfer Kinetics of Ferrocenemethanol in Dimethyl Sulfoxide− Water Mixtures. *J. Phys. Chem. B* **2002**, *106*, 1392−1398.
(31) Wang, L.; Wang, Y.; Zhuang, Q. Simple self-referenced ratiometric electrochemical sensor for dopamine detection using electrochemically pretreated glassy carbon electrode modified by acid-treated multiwalled carbon nanotube. *J. Electroanal. Chem.* **2019**, *851*, 113446.
(32) Wong, E. L.; Mearns, F. J.; Gooding, J. J. Further development of an electrochemical DNA hybridization biosensor based on long-range electron transfer. *Sens. Actuators, B* **2005**, *111*−*112*, 515−521.
(33) Martin, E. T.; McGuire, C. M.; Mubarak, M. S.; Peters, D. G. Electroreductive remediation of halogenated environmental pollutants. *Chem. Rev.* **2016**, *116*, 15198−15234.
(34) Pasciak, E. M.; Sengupta, A.; Mubarak, M. S.; Raghavachari, K.; Peters, D. G. Electrochemical reduction of 2-chloro-N-phenylacetamides at carbon and silver cathodes in dimethylformamide. *Electrochim. Acta* **2014**, *127*, 159−166.
(35) Couto Petro, A. G.; Mubarak, M. S.; Peters, D. G. Electrochemical reduction of 2-halo-N-phenylacetamides at glassy carbon cathodes in dimethylformamide. *J. Electroanal. Chem.* **2019**, *840*, 456−461.
(36) Strawsine, L. M.; Sengupta, A.; Raghavachari, K.; Peters, D. G. Direct reduction of alkyl monohalides at silver in dimethylformamide: effects of position and identity of the halogen. *ChemElectroChem* **2015**, *2*, 726−736.
(37) Cleary, J. A.; Mubarak, M. S.; Vieira, K. L.; Anderson, M. R.; Peters, D. G. Electrochemical Reduction of Alkyl-Halides at Vitreous Carbon Cathodes in Dimethylformamide. *J. Electroanal. Chem.* **1986**, *198*, 107−124.
(38) Klein, M.; Waldvogel, S. R. Counter Electrode Reactions-Important Stumbling Blocks on the Way to a Working Electro-organic Synthesis. *Angew. Chem. Int. Ed.* **2022**, *61*, No. e202204140.
(39) Dorr, M.; Hielscher, M. M.; Proppe, J.; Waldvogel, S. R. Electrosynthetic Screening and Modern Optimization Strategies for Electrosynthesis of Highly Value-added Products. *ChemElectroChem* **2021**, *8*, 2620−2629.

https://doi.org/10.1021/acsmeasuresciau.3c00022
ACS Meas. Sci. Au 2023, 3, 371−379